



HAL
open science

Nuclear Structure with Discrete Non-Orthogonal Shell-Model: new frontiers

Dao Duc, Frederic Nowacki

► **To cite this version:**

Dao Duc, Frederic Nowacki. Nuclear Structure with Discrete Non-Orthogonal Shell-Model: new frontiers. *Physical Review C*, 2022, *Physical Review C*, 105 (5), pp.054314. 10.1103/PhysRevC.105.054314. hal-03593473v3

HAL Id: hal-03593473

<https://hal.science/hal-03593473v3>

Submitted on 4 May 2022

HAL is a multi-disciplinary open access archive for the deposit and dissemination of scientific research documents, whether they are published or not. The documents may come from teaching and research institutions in France or abroad, or from public or private research centers.

L'archive ouverte pluridisciplinaire **HAL**, est destinée au dépôt et à la diffusion de documents scientifiques de niveau recherche, publiés ou non, émanant des établissements d'enseignement et de recherche français ou étrangers, des laboratoires publics ou privés.



Distributed under a Creative Commons Public Domain Mark 4.0 International License

Nuclear Structure with Discrete Non-Orthogonal Shell Model: new frontiers

D. D. Dao¹ and F. Nowacki¹

¹*Université de Strasbourg, CNRS, IPHC UMR7178, 23 rue du Loess, F-67000 Strasbourg, France*

(Dated: May 4, 2022)

We present developments and applications for the diagonalization of shell-model hamiltonians in a discrete non-orthogonal basis (DNO-SM). The method, and its actual numerical implementation **CARINA**, based on mean-field and beyond-mean field techniques has already been applied in previous studies and is focused on basis states selection optimization. The method is benchmarked against a full set of *sd* shell exact diagonalizations, and is applied for the first time to the heavy deformed ²⁵⁴No nucleus.

PACS numbers: 23.20.Js, 23.20.Lv, 27.60.+j, 25.85.Ca

I. INTRODUCTION

In the recent decades, the advent of radioactive beam factories associated with developments of more sophisticated experimental methods has enabled to discover new manifestations of many-body nuclear dynamics in many places of the nuclear chart. New phenomena like halo systems, two-proton radioactivity, occurrence of new magic numbers, vanishing of shell closures, soft dipole modes, or even searches for superheavy nuclei have been observed and have stimulated the continuous developments and improvements of theoretical methods in order to interpret such phenomena.

Among the various theoretical frameworks available, the Shell-Model (SM) or Configuration Interaction (CI), either in its no-core or valence space implementations, has always been one of the most powerful methods in the description of quantum nuclear systems [1, 2], in particular with the numerical development of efficient diagonalization codes which have opened the era of the so-called "Large Scale Shell-Model calculations" for light and medium-mass nuclei up to $A \sim 150$ [3–8] and have become the method of choice to explain the observed nuclear phenomena, guide experimental programs, and not the least, allowed for a deeper understanding of many astrophysical objects and processes in which exotic nuclei often play the key role. However, its success was always minored by the exponential growth of the systems basis involved. At the same time, variational methods with symmetry breaking and restoration have also shown great success for decades and have proven to a certain extent to be applicable over the nuclear chart from the lightest nuclear systems to the most heavy ones [9–11].

Although these methods provide distinct description, the merging of the mean-field techniques within the shell-model formalism has already been developed and studied in the literature in the past, starting from the pioneering work of Ripka [12, 13], later followed by the different **VAMPIR** implementations [14, 15]. One of the major achievements up to now was proposed by the Tokyo group with the Monte Carlo Shell-Model [16–18]. And more recently several implementations were used, either in an punctual manner [19, 20] or in a more ambitious

scale with the recent development of the **TAURUS** numerical suite [21–23].

In the present work, we present the formalism of the Discrete Non-Orthogonal Shell-Model (DNO-SM) and its associated numerical implementation **CARINA**. The DNO-SM amounts to diagonalize valence shell-model hamiltonians in a non-orthogonal basis with the use of beyond-mean-field techniques. The detailed framework is exposed in the next section and applications to *sd* shell nuclei in comparison with exact diagonalisations are discussed in section III. The final section exposes an application to a very heavy system in the ²⁵⁴No case.

II. THEORETICAL FRAMEWORK

A. Shell Model formulation revisited

1. The diagonalization dilemma

The ultimate question in the Shell Model, once a physically meaningful valence space \mathcal{E} is equipped together with the associated effective interaction $\hat{\mathcal{V}}$ for the problem at hand, is to tackle the secular equation

$$\hat{\mathcal{H}}|\Psi\rangle = E|\Psi\rangle \quad (1)$$

where $\hat{\mathcal{H}}$ represents the effective Hamiltonian composed of $\hat{\mathcal{V}}$ and a one-body single-particle energy $\{e_i\}$ part

$$\hat{\mathcal{H}} = \sum_{i \in \mathcal{E}} e_i a_i^\dagger a_i + \frac{1}{4} \sum_{ijkl \in \mathcal{E}} \langle ij|\hat{\mathcal{V}}|kl\rangle a_i^\dagger a_j^\dagger a_l a_k. \quad (2)$$

$\{a_i^\dagger\}$ and $\{a_i\}$ are creation and annihilation operators satisfying the common anti-commutation rules for fermionic systems.

By defining a set of basis states $\mathcal{B} = \{|\phi_m\rangle, m \in \mathbb{N}\}$ constructed from the single-particle spherical oscillator valence space \mathcal{E} with which we can write the eigenstate $|\Psi\rangle$ as

$$|\Psi\rangle = \sum_{m=1}^{\dim(\mathcal{B})} c_m |\phi_m\rangle, \quad (3)$$

the classic Shell Model resolution of (1) then amounts to addressing the eigenvalue problem

$$\sum_{m=1}^{\dim(\mathcal{B})} \mathcal{H}_{m'm} c_m = E c_{m'} \quad (4)$$

by an exact diagonalization of the Hamiltonian matrix $\mathcal{H}_{m'm} = \langle \phi_{m'} | \hat{\mathcal{H}} | \phi_m \rangle$ in the model space $\mathcal{H} = \overline{\text{Span } \mathcal{B}}$. Although spectacular designs of Shell Model codes have been achieved [1] to reach space dimensions larger and larger, it is still an inherent problem that makes difficult to extend the Shell Model applicability into heavier mass nuclei. To deal with this dilemma, we look for a replacement of \mathcal{B} with a different family of basis states. The existence of such basis takes the root in the original idea of the Generator Coordinate Method (GCM) first proposed in Refs. [24, 25]. As we shall discuss in the following, it can be however viewed in an independent status with respect to the GCM, thanks to the work of the authors in Ref. [26].

2. Discrete non-orthogonal basis

The starting point of the GCM is the hypothesis that one can find a family of states depending on the continuous (generator) coordinate(s) q

$$\Gamma = \{ |\Phi(q)\rangle \mid q \in \mathbb{R} \} \quad (5)$$

so that the latter forms a model subspace $\mathcal{H}_q = \overline{\text{span } \Gamma} \subseteq \mathcal{H}$ following the nature of the coordinate(s) q that we choose in the generation of Γ . The core of our presentation of \mathcal{H}_q relies on the following existence theorem first noticed in Ref. [26]. Suppose \mathcal{H}_q is a separable Hilbert subspace, i.e. $\mathcal{H}_q \subseteq \mathcal{H} \subset \mathcal{L}^2$ where \mathcal{L}^2 denotes the full Hilbert space associated with the space of square integrable functions, the separability property of \mathcal{H}_q implies the existence of a countable family

$$\Gamma_0 = \{ |\Phi(q_i)\rangle \mid i \in \mathbb{N} \} \subset \Gamma \quad (6)$$

which is in general skew or non-orthogonal set of states with the property $\mathcal{H}_q = \text{span } \Gamma_0$ (cf. the detailed demonstration given in Appendix of Ref. [26]). This enables us to tackle now the diagonalization of $\hat{\mathcal{H}}$ in the subspace \mathcal{H}_q represented by the discrete non-orthogonal basis set Γ_0 . Indeed, by expressing the eigenstate $|\Psi\rangle$ as

$$|\Psi\rangle = \sum_{i=0}^{\infty} f(q_i) |\Phi(q_i)\rangle, \quad (7)$$

the projection of (1) in \mathcal{H}_q becomes equivalent to the generalized eigenvalue problem

$$\sum_{i=0}^{\infty} \left[\mathcal{H}(q_i', q_i) - E \mathcal{N}(q_i', q_i) \right] f(q_i) = 0 \quad (8)$$

where $\mathcal{O}(q_i', q_i) = \langle \Phi(q_i') | \hat{\mathcal{O}} | \Phi(q_i) \rangle$ ($\hat{\mathcal{O}} = \hat{\mathcal{H}}, \mathbf{1}$) are the Hamiltonian and norm matrix elements and $f(q_i)$ the expansion coefficient.

Therefore, instead of using the basis \mathcal{B} spanning the full model space \mathcal{H} , the above presented theorem on the existence (not necessarily unique) of a discrete non-orthogonal basis set of $\hat{\mathcal{H}}$ suggests that:

1. the diagonalization of $\hat{\mathcal{H}}$ in \mathcal{H}_q becomes “exact” when $\mathcal{H}_q = \mathcal{H}$, which means the coordinate(s) q must be chosen so as to “exhaust” in some way the space \mathcal{E} ;
2. the truncation of the infinite countable set Γ_0 could be done in a variational way such that the finite sum

$$|\Psi\rangle \approx \sum_{i=0}^n f(q_i) |\Phi(q_i)\rangle \quad (9)$$

yields an optimal approximation.

Whether we are able to choose q to fulfil the condition $\mathcal{H}_q = \mathcal{H}$ can be verified a posteriori. What needed is then an efficient truncation method of Γ_0 , which we shall address now.

3. Truncation method with the minimization technique

The existence theorem as presented previously has enabled us to transform the classic Shell Model eigenvalue problem (4), formulated in the orthonormal basis \mathcal{B} , into the generalized one (8) through the discrete non-orthogonal basis Γ_0 . As noted earlier by the authors of Ref. [26], the minimization technique originally proposed by E. Caurier in Ref. [27] provides an iterative prescription to truncate Γ_0 in a variational way.

It proceeds as follows [27]: “the first point q_0 is the one such that $|\Phi(q_0)\rangle$ minimizes the energy. The second point q_1 is chosen in such a way that the energy obtained from diagonalizing the Hamiltonian in the 2-dimensional space spanned by $|\Phi(q_0)\rangle$ and $|\Phi(q_1)\rangle$ be a minimum. One proceeds in the same way to determine the third basis vector $|\Phi(q_2)\rangle$ etc...”.

The technique was however implemented only in toy model examples of Hydrogen atom in molecular physics (cf. e.g. [28]) and has never been considered in realistic nuclear structure calculations. Therefore, instead of the conventional problem represented by $(\hat{\mathcal{H}}, \mathcal{H}, \mathcal{B})$, our current work exploits fully this technique for the first time in the Shell Model framework formulated in terms of $(\hat{\mathcal{H}}, \mathcal{H}_q, \Gamma_0)$. This resulting model will be from now on referred to as *Discrete Non-Orthogonal Shell Model* (DNO-SM).

To be now more precise in the practical realization of the DNO-SM, we assume that the Projected Constrained Hartree-Fock (PCHF) approach provides us with a basis generation method which will be our focus in the next

subsection. However, before going further, let us note that, the above proposed technique suggested to minimize one state at a time. More generally in order to cover broader physical situations such as nuclear coexistences where the potential energy surface may exhibit several local minima or when states are not of collective nature, it may be more preferable to obtain various excited states by a single minimization. A generalization to deal with the minimization of many states simultaneously shall be presented.

B. Projected constrained Hartree-Fock basis

Having introduced the general framework of our approach to the dimensionality problem encountered in the classic Shell Model, we present now the construction of the many-body basis in the DNO-SM. The choice of degrees of freedom here is important to take into account correlations as much as possible in the generation of the basis. This should be inferred on physical grounds. Moreover, the many-body basis must conserve important symmetries of the effective Hamiltonian, in particular, the cases associated with conserved quantities such as the angular momentum and particle numbers. Such basis could be built upon the Constrained Hartree-Fock (CHF) method which relies on the rotational symmetry breaking at the mean field to incorporate deformations. A projection onto good angular momentum can be applied later before proceeding to the full diagonalization.

A Hartree-Fock (HF) state $|\Phi(q)\rangle = \prod_{i=1}^A a_i^\dagger |0\rangle$ for a nucleus of A -particles is obtained from CHF calculations under the conditions

$$\frac{1}{2} \langle \Phi | \hat{Q}_{\lambda\mu} + (-)^\mu \hat{Q}_{\lambda-\mu} | \Phi \rangle = Q_{\lambda\mu}, \quad (10)$$

$$\langle \Phi | \hat{J}_m | \Phi \rangle = \langle \hat{J}_m \rangle \quad (m = x, z), \quad (11)$$

where $\hat{Q}_{\lambda\mu} = r^\lambda Y_{\lambda\mu}(\theta, \varphi)$ is the multipole operator expressed in terms of the spherical harmonics $Y_{\lambda\mu}$ and \hat{J}_m the components of the total angular momentum operator $\hat{\mathbf{J}}$. Here $Q_{\lambda\mu}$ and $\langle \hat{J}_m \rangle$ are desired constraining expectation values. Our numerical implementations of constrained HF calculations follow the standard modified Broyden method as described in Refs. [29–31]. Furthermore, to ensure the correct constraining value along the iterative HF process, we use the augmented Lagrange method proposed in Ref. [32].

Once this is done, the resulting HF state is projected onto good angular momentum J through the usual procedure using the projection operator [13, 33]

$$\mathcal{P}_{MK}^J(A) = \frac{2J+1}{4\pi^2(3-(-)^A)} \times \int_0^{2\pi} d\alpha \int_0^\pi d\beta \int_0^{\gamma_{\max}} d\gamma \mathcal{D}_{MK}^{J*}(\alpha, \beta, \gamma) \hat{R}(\alpha, \beta, \gamma), \quad (12)$$

where $\gamma_{\max} = (3 - (-)^A)\pi$, $\hat{R}(\alpha, \beta, \gamma)$ and $\mathcal{D}_{MK}^{J*}(\alpha, \beta, \gamma)$ denote the rotation operator and the Wigner matrix [34]. The case of $\gamma_{\max} = 4\pi$ corresponds to a HF state describing odd systems. Thus we have included the dependence of the projection operator on the mass number A for convenience. This provides us a family of PCHF states characterized by the angular momentum projection onto the intrinsic axis $|K| \leq J$ and the coordinate q for a given J

$$\Gamma = \{\mathcal{P}_{MK}^J(A)|\Phi(q)\rangle \mid q \in \mathbb{R}\} \quad (13)$$

with which we can now formulate the DNO-SM's working equations.

The HF procedure to generate deformed Slater determinants in the construction of DNO-SM basis is implemented to treat both odd- and even-nuclei without further assumptions. More specifically, we do not impose any self-consistent symmetries (e.g. no time-reversal, no parity conservation) at the HF mean field to exploit at best what is offered by the single-particle valence space \mathcal{E} . The construction of DNO-SM basis for odd nuclei is done via the constrain of angular momentum components \hat{J}_m ($m = x, z$) which, as we will show later, can provide a very good many-body basis for such nuclei. The formal aspect of this approach to treat odd-mass nuclei has been pointed out in Ref. [35]. More recently, the theoretical demonstration in the Hartree-Fock-Bogoliubov framework is described in Ref. [36].

Since there is no self-consistent symmetries adopted here, the angular momentum projection demands to perform the integration over Euler angles $\Omega = (\alpha, \beta, \gamma)$ in full intervals without restrictions. To do so, we have developed an analytical formula that performs an exact integration over (α, γ) whose derivation is presented in Appendix B. The integration over β is done numerically using the Gauss-Legendre quadrature rule.

C. DNO-SM formalism

1. Secular equation in non-orthogonal PCHF basis

Let us start with the ansatz (7) where we specify the eigenstate of $\hat{\mathcal{H}}$ by $|\alpha JM\rangle$ of good total angular momentum J , its projection M in the laboratory frame and an index α labelling indices of corresponding energy levels and other quantum numbers. In terms of the PCHF states $\mathcal{P}_{MK}^J|\Phi(q)\rangle \in \Gamma_0 \subset \Gamma$, it is given by

$$|\alpha JM\rangle = \sum_{q,K} f_\alpha^{(J)}(q; K) \mathcal{P}_{MK}^J|\Phi(q)\rangle. \quad (14)$$

To simplify the notation, we omit the dependence on mass number A in the projection operator \mathcal{P}_{MK}^J and q is understood to take discrete values. The projected equation (8) then becomes

$$\sum_{q,K} \left[\mathcal{H}_{K',K}^J(q', q) - E_\alpha^{(J)} \mathcal{N}_{K',K}^J(q', q) \right] f_\alpha^{(J)}(q; K) = 0 \quad (15)$$

where the Hamiltonian and the norm matrix elements $\mathcal{O}_{K'K}^{(J)}(q', q) = \langle \Phi(q') | \hat{\mathcal{O}} \mathcal{P}_{K'K}^J | \Phi(q) \rangle$ (with $\hat{\mathcal{O}} = \hat{\mathcal{H}}, \mathbf{1}$) are evaluated through a three-fold integration over Euler angles $\Omega = (\alpha, \beta, \gamma)$

$$\mathcal{O}_{K'K}^{(J)}(q', q) = \frac{2J+1}{4\pi^2(3-(-)^A)} \times \int d\Omega \mathcal{D}_{MK}^{J*}(\Omega) \langle \Phi(q') | \hat{\mathcal{O}} \hat{R}(\Omega) | \Phi(q) \rangle. \quad (16)$$

The core of (16) is in the evaluation of the kernels $\langle \Phi(q') | \hat{\mathcal{O}} \hat{R}(\Omega) | \Phi(q) \rangle$ for given pair of Slater determinants. For these calculations, we use the minor formula as presented in Ref. [37]. This is given in Appendix A. The matrix element $\mathcal{O}_{K'K}^{(J)}(q', q)$ obtained from the Euler angles integration is then presented in Appendix B.

The treatment of the generalized eigenvalue problem (15) has been well documented in the framework of the generator coordinate method (see e.g. Refs. [38–40]). We follow the standard technique that begins with the determination of the natural eigenbasis functions $u_i^{(J)}(q; K)$ of the norm matrix

$$\sum_{q,K} \mathcal{N}_{K'K}^J(q', q) u_i^{(J)}(q; K) = \eta_i^{(J)} u_i^{(J)}(q'; K'). \quad (17)$$

By retaining only positive norm eigenvalues that we denote by $\{\eta_i^{(J)} > 0, i \in \mathbb{N}\}$, the so-called natural state characterized by the corresponding norm eigenvalue $\eta_i^{(J)}$ is defined as

$$|\eta_i^{(JM)}\rangle = \frac{1}{\sqrt{\eta_i^{(J)}}} \sum_{q,K} u_i^{(J)}(q; K) \mathcal{P}_{MK}^J | \Phi(q) \rangle, \quad (18)$$

$$\langle \eta_{i'}^{(JM)} | \eta_i^{(JM)} \rangle = \delta_{i'i}$$

and satisfies the orthogonality condition. This natural basis allows to transform the projected equation in the non-orthogonal PCHF basis onto the usual eigenvalue problem of the form

$$\sum_{i'} \mathcal{H}_{i'i}^{(J)} g_{i'}^{(J)} = E_\alpha^{(J)} g_i^{(J)} \quad (19)$$

where the Hamiltonian matrix now is expressed between orthogonal natural basis states $\{|\eta_i^{(JM)}\rangle\}$

$$\mathcal{H}_{i'i}^{(J)} = \frac{1}{\sqrt{\eta_{i'}^{(J)} \eta_i^{(J)}}} \sum_{q', K', qK} u_{i'}^{(J)*}(q'; K') \times \mathcal{H}_{K'K}^J(q', q) u_i^{(J)}(q; K). \quad (20)$$

The nuclear state $|\alpha JM\rangle$ is thus a linear superposition in the natural basis

$$|\alpha JM\rangle = \sum_i g_i^{(J)} |\eta_i^{(JM)}\rangle \quad (21)$$

with the transformation onto the non-orthogonal PCHF basis expressed through the expansion coefficient $f_\alpha^{(J)}(q; K)$ of (14)

$$f_\alpha^{(J)}(q; K) = \sum_i \frac{g_i^{(J)}}{\sqrt{\eta_i^{(J)}}} u_i^{(J)}(q; K). \quad (22)$$

One can notice that $f_\alpha^{(J)}(q; K)$ is not properly normalized and does not represent the probability amplitude of finding a given configuration of Γ_0 . To be able to analyze the content of the nuclear states, we can define the normalized probability amplitude to find a component $\mathcal{P}_{MK}^J | \Phi(q) \rangle$ in the state $|\alpha JM\rangle$ by [38, 41]

$$\mathcal{M}_\alpha^{(J)}(q; K) = \sum_{q', K'} [\hat{\mathcal{N}}^{1/2}]_{K'K}^{(J)}(q', q) f_\alpha^{(J)}(q'; K'). \quad (23)$$

The corresponding probability to find the intrinsic angular momentum component K or the component q in the state $|\alpha JM\rangle$ is respectively given by

$$\mathcal{P}_\alpha^{(J)}(K) = \sum_q \left| \mathcal{M}_\alpha^{(J)}(q; K) \right|^2, \quad (24)$$

$$\mathcal{P}_\alpha^{(J)}(q) = \sum_K \left| \mathcal{M}_\alpha^{(J)}(q; K) \right|^2,$$

with the normalization relation

$$\sum_K \mathcal{P}_\alpha^{(J)}(K) = \sum_q \mathcal{P}_\alpha^{(J)}(q) = 1. \quad (25)$$

2. Truncation of the PCHF basis with the generalized minimization technique

We come now to the truncation of the discrete family Γ_0 with the minimization technique. The idea about how to choose states of Γ_0 is quite straightforward. That is, applying to the present case including the angular momentum projection, based on the selection of discrete values of the coordinate(s) q which minimizes the energy, i.e. we let the Hamiltonian itself to choose what is the best state from a variational viewpoint. Furthermore, it is implicitly understood that the ground state or an excited state has to be chosen beforehand. Then the following iterative procedure can be implemented:

- 1) Fix the state $E_\alpha^{(J)}$ to be minimized with α indexing energy levels;
- 2) Define a searching region of the coordinate(s) q ;
- 3) Start from the first point which can be chosen as the HF minimum;
- 4) Solve the projected Shell Model circular equation (15) over the whole searching region of q to find the second state and proceed the same way in next iterations until the convergence of $E_\alpha^{(J)}$.

More precisely, the convergence criterion is defined by the absolute energy gain $\Delta E_\alpha^{(J)}(k) = E_\alpha^{(J)}(k) - E_\alpha^{(J)}(k-1)$ at the iteration number k . If $\Delta E_\alpha^{(J)}(k) > \epsilon > 0$ we keep the CHF state, otherwise it is not retained. The minimization will stop when no more states are found in the searching region.

In practice, we observe that fixing (α, J) will exclude in the minimization the states of Γ_0 which could be relevant for an other state (α', J') . Hence, small components of the wave functions could be missed whereas the overall spectrum remains well described. The key point is thus, minimizing as many excited states at the same time as possible will eventually lead to the improvement of one and another mutually and also the ground state. This idea leads us to generalize the above iterative procedure in the following way: we let the minimization process to determine not only the coordinate(s) q but also the state (α, J) that gains the most energy at a given iteration. This is done by comparing the energy differences $\{\Delta E_\alpha^{(J)}\}$ for every state (α, J) in a given set of nuclear states which we want to describe. The procedure then continues until we find no more states satisfying the condition $\max\{\Delta E_\alpha^{(J)}\} > \epsilon$, which defines the convergence criterion in this scheme. We will comment on the choice of ϵ in the following.

The minimization procedure as such requires an organizational scheme of partitioning the coordinate(s) q , which form in general a multi-dimensional surface. Although it is possible to determine all of them simultaneously in principle, it might not be necessary to do so. The reason is that, as a consequence of the existence theorem, different countable sets $\Gamma_0 \subset \Gamma$ could be qualified as basis for \mathcal{H}_q . In this work, we define the following organization of the coordinate(s) q . Only the deformation parameters $Q_{\lambda\mu}$ are determined from the minimization process. The cranking components $\langle \hat{J}_m \rangle$ ($m = x, z$) are not. Instead, they are fixed in advance. That is, we perform the minimization in the deformation surface $\{Q_{\lambda\mu}\}$ associated to each value of $\langle \hat{J}_m \rangle = J_m^{(1)}, J_m^{(2)}, J_m^{(3)}, \dots$ ordered from input.

3. Choice of the coordinate(s) q

In order to generate Γ_0 , in this present work, we limit ourselves to quadrupole deformations (axial and triaxial) as the common choice of generator coordinates for triaxial systems [41], whose expectation values in a HF state $|\Phi\rangle$ are denoted by Q_{20}, Q_{22} respectively

$$Q_{20} = \sqrt{\frac{16\pi}{5}} \sum_{\tau=p,n} e_{mass}^{(\tau)} \langle \Phi | \hat{Q}_{20}^{(\tau)} | \Phi \rangle \quad (26)$$

$$Q_{22} = \sqrt{\frac{8\pi}{5}} \sum_{\tau=p,n} e_{mass}^{(\tau)} \langle \Phi | (\hat{Q}_{2-2}^{(\tau)} + \hat{Q}_{22}^{(\tau)}) | \Phi \rangle. \quad (27)$$

In this particular case, we use the usual Hill-Wheeler (β, γ) parameters [42] which are related to (Q_{20}, Q_{22}) through the total quadrupole moment $Q = \sqrt{Q_{20}^2 + Q_{22}^2}$

$$\beta = \frac{b^2 Q \sqrt{5\pi}}{3r_0^2 A^{5/3}}, \quad \gamma = \arctan\left(\frac{Q_{22}}{Q_{20}}\right) \quad (28)$$

where b^2 (in fm²) is the harmonics oscillator parameter [43–45]

$$b^2 = \frac{41.4}{45A^{-1/3} - 25A^{-2/3}}, \quad (29)$$

and A and $r_0 = 1.2$ (in fm) are the nuclear mass number and radius parameter.

Within the shell-model formalism, the use of valence spaces and truncation of the Hilbert space implies the need of effective hamiltonians as well as effective operators. Effective operators can be derived by Many-Body Perturbation Theory [46] but quadrupole operators are usually renormalized with the use of an effective charge. The effective charge have been defined by several authors, we use here the notation defined in Ref. [44]:

$$e_{el}^{(p)} = (1 + \chi_p)e, \quad e_{el}^{(n)} = \chi_n e \quad (30)$$

with χ being the electric polarization charge. χ value is intimately connected to the valence space used and can be derived by Many-Body Perturbation Theory [46] and is shell dependent but for $0\hbar\omega$ spaces, the microscopic Dufour-Zuker [47] $\chi_p = 0.31$, $\chi_n = 0.46$ are standard values. Finally, for the mass quadrupole operators, we will use

$$e_{mass}^{(p)} = e_{mass}^{(n)} = (1 + \chi_p + \chi_n)e \quad (31)$$

to be consistent with the deformation parameters defined above.

III. BENCHMARK AND COMPARISON IN SD NUCLEI

A. Even nuclei

To assess the quality of the PCHF basis Γ_0 against the oscillator one in the classic Shell Model, we perform a systematic comparison of two models in even sd nuclei using the USDB effective interaction [48].

In the first series of calculations shown in Table II, to see the overall performance of our minimization method, we compare the ground state and the first excited states $2_1^+, 4_1^+$ energies as well as the corresponding $E2$ -transition probabilities for Neon, Magnesium, Silicon and Argon even-even isotopes. These calculations are performed using: i) the common set of states $J_\alpha \in \{0_1, 2_{1,2}, 4_1, 8_1, 12_1, 16_1\}$ whenever possible; ii) practically the same (β, γ) mesh for all considered nuclei (cf. Table I); iii) the same set of cranking components

$\langle \hat{J}_z \rangle \in \{-2, -4, -8, -12, -16\}$ and iv) the same number of integration points in Angular Momentum Projection, namely, 11 points for the analytical integration over the angles $\alpha, \gamma \in [0, 2\pi]$ and 20 Gauss–Legendre quadrature points for the integration over the angle $\beta \in [0, \pi]$. After a first round of minimization to find non- cranked CHF states over the range $\gamma \in [0^\circ, 60^\circ]$ discretized into a one-dimensional mesh of N_g points, the minimization procedure is then iterated for each above-mentioned cranking components $\langle \hat{J}_z \rangle$.

As we can see in Table II, the agreement between two models is excellent for both relative energies and $E2$ –transition probabilities, indicating that the wave functions have already converged for the considered states. The number of CHF basis states found by the minimization process is relatively small at the beginning and the end of the shell and increases as we go to nuclei at mid shell. Such are the cases of deformed open shell nuclei ^{24}Mg , ^{28}Si which seemingly require more basis states to capture correlations in the mixing than in others. In the present calculations, a similar trend is exhibited in the ground state binding energy difference (of order $\sim 0.1 - 1.0$ MeV) with respect to the exact result (shown in Figure 1). There are two possible reasons for this underbinding:

- Our minimization technique builds up the many-body basis based on a finite set of states preliminarily defined, in the present case, i.e. the set $J_\alpha \in \{0_1, 2_{1,2}, 4_1, 8_1, 12_1, 16_1\}$, hence, indirectly omits basis states possibly relevant for other states not included in the set. Therefore, the representation of the effective Hamiltonian in the truncated basis Γ_0 is not fully complete as the construction is under way. This is in contrast to the full SM diagonalization in the oscillator basis because all many-body matrix elements of the effective Hamiltonian are available once the valence space is defined.
- The second reason may be related to the choice of the coordinate(s) q . Here, the question that arises is which q to be used to ensure *a priori* the full representation of the effective Hamiltonian.

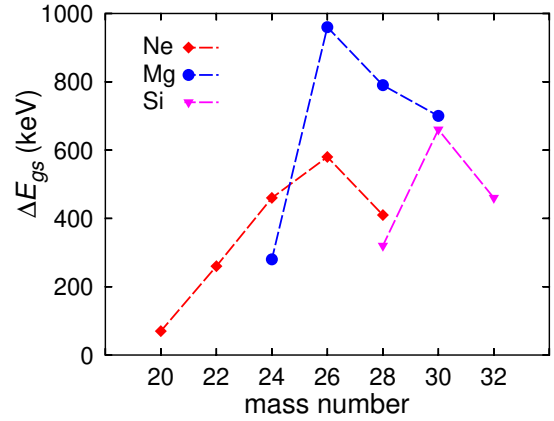


Figure 1: Energy difference (in keV) between the DNO-SM and the exact SM diagonalizations in the ground state of even Ne, Mg and Si isotopes from Table II.

Table I: Discretization of the (β, γ) plane for minimization procedure for selected sd nuclei using the USDB effective interaction. The Hartree-Fock minimum energy (E_{HF}) and corresponding mass quadrupole parameters ($\beta_{\text{min}}, \gamma_{\text{min}}$) are also given. γ_{min} is in degree. The effective charges for protons and neutrons are $e_{\text{mass}}^{(p)} = e_{\text{mass}}^{(n)} = 1.77$ (see EQ.(31)).

β	N_b	N_g	nucleus	β_{min}	$\gamma_{\text{min}} (^{\circ})$	E_{HF} (MeV)
[0.1, 0.7]	11	9	^{20}Ne	0.527	0.0	-36.404
			^{22}Ne	0.498	0.0	-53.474
[0.1, 0.53]	11	9	^{24}Ne	0.313	23.8	-66.225
			^{26}Ne	0.247	0.0	-77.258
			^{28}Ne	0.198	0.0	-83.441
			^{24}Mg	0.499	12.0	-80.965
			^{26}Mg	0.395	34.0	-98.887
			^{28}Mg	0.325	0.0	-115.625
[0.1, 0.48]	7	9	^{30}Mg	0.212	0.0	-126.735
			^{28}Si	0.425	60.0	-130.021
			^{30}Si	0.285	46.8	-148.238
			^{32}Si	0.221	60.0	-166.344
			^{32}S	0.0	-	-176.393
			^{34}S	0.152	60.0	-198.097
			^{36}Ar	0.199	60.0	-226.611

B. Detailed analysis of ^{24}Mg

In the second series of calculations, we investigate the specific case of ^{24}Mg , which is a typical example of deformed nuclei in the sd shell. This nucleus was extensively studied in the past within various approaches [19, 38, 39, 49, 50]. It is well established that it has a triaxial shape in its ground state with a rotational

Table II: Systematics comparison of the diagonalization in the model spaces \mathcal{H}_q and \mathcal{H} of the Shell Model in even sd nuclei. The absolute ground state energy E_{gs} and relative energies of the first 2^+ and 4^+ are given in MeV. Their reduced transition probabilities $B(E2; 2_1^+ \rightarrow 0_1^+)$ and $B(E2; 4_1^+ \rightarrow 2_1^+)$ are in $e^2 \cdot \text{fm}^4$ unit. N_q denotes the number of CHF states $|\Phi(q)\rangle$ found with the minimization procedure.

nucleus	\mathcal{H}_q			\mathcal{H}		E_{gs} (MeV)		$B(E2; 2_1^+ \rightarrow 0_1^+)$		$B(E2; 4_1^+ \rightarrow 2_1^+)$	
	N_q	2_1^+	4_1^+	2_1^+	4_1^+	\mathcal{H}_q	\mathcal{H}	\mathcal{H}_q	\mathcal{H}	\mathcal{H}_q	\mathcal{H}
^{20}Ne	16	1.76	4.14	1.75	4.18	-40.40	-40.47	47.0	46.9	56.3	55.3
^{22}Ne	41	1.37	3.39	1.36	3.36	-57.32	-57.58	48.1	46.9	64.0	63.3
^{24}Ne	39	2.13	4.01	2.11	3.99	-71.26	-71.72	38.8	38.7	31.9	31.3
^{26}Ne	26	2.12	3.72	2.06	3.51	-80.98	-81.56	39.6	38.5	37.8	33.8
^{28}Ne	12	1.55	2.82	1.62	2.99	-86.13	-86.54	34.3	34.1	32.7	30.7
^{24}Mg	42	1.52	4.37	1.50	4.37	-86.82	-87.10	76.1	74.4	99.1	97.5
^{26}Mg	50	1.80	4.36	1.89	4.36	-104.56	-105.52	66.1	65.2	27.5	18.0
^{28}Mg	50	1.40	4.07	1.52	4.17	-119.71	-120.50	62.9	60.2	75.7	67.5
^{30}Mg	21	1.50	3.89	1.59	3.89	-129.77	-130.47	53.0	49.1	39.6	32.5
^{28}Si	71	2.12	4.78	1.93	4.61	-135.54	-135.86	77.4	77.9	106.8	109.6
^{30}Si	46	2.25	5.59	2.26	5.33	-154.09	-154.75	46.9	45.9	54.0	15.8
^{32}Si	43	1.99	5.79	2.05	5.88	-170.06	-170.52	41.1	42.5	66.9	65.2
^{32}S	50	2.05	4.55	2.16	4.65	-182.10	-182.45	48.0	46.9	69.2	66.8
^{34}S	36	2.01	4.66	2.13	4.83	-202.08	-202.50	38.3	36.0	51.7	48.0
^{36}Ar	12	1.81	4.46	1.82	4.49	-230.22	-230.28	50.4	50.6	63.2	62.9

band built on top. Moreover, the triaxiality manifests itself in the existence of the so-called γ -band that was experimentally observed. In order to examine whether our method is able to correctly describe these features, we explore different minimization schemes as proposed in IIC 2.

To fix ideas, let us first mention that the present calculations of ^{24}Mg as shown in Figure 3 are performed using the same (β, γ) discretization as in Table I and the cranking components $\langle \hat{J}_z \rangle \in \{0, -2, -3, -4, -5\}$. Results reported in the figures 3b), 3c) and 3d) are obtained from the ground-state and many states minimizations in comparison with the full mesh diagonalization 3e) and the exact SM diagonalization 3f). The searching domain for minimizations is also the dimension of the full mesh calculation which is *a priori* $7 \times 9 \times 5 = 315$. In practice, our Hartree-Fock calculations found 277 converged solutions.

From Figure 3 the first thing we note is that Angular Momentum Projection from the HF minimum gives already very good intraband transitions. In contrast, the interband transitions $BE(2; 2_2^+ \rightarrow 2_1^+)$ or $BE(2; 6_1^+ \rightarrow 5_1^+)$ which reflect the K -mixing of the two bands are significantly underestimated. In minimizing the ground state alone, the interband transitions are considerably improved and consistent with the exact SM result using only 6 basis states. This means we have already the right wave functions with the mixing of a few number of CHF states, even though about ~ 600 keV is still missing in the ground state binding. Carrying out the same min-

imization of the ground state until no more CHF basis vectors are found in the full mesh, we obtain 39 states that perfectly reproduce the exact SM result. This calculation also confirms that in the ground-state minimization, 6 CHF vectors is enough to have good solutions in this nucleus.

Now to see whether we can improve further by minimizing many states at the same time, as shown in the figure 3d), we find 55 CHF states that provide an overall better energy spectra than the ground-state minimization but does not change much the picture. The excited states in the figure 3d) are slightly more compressed. This effect, as shown in Figure 5, can be traced back to the addition of cranked CHF states which are known to stretch down the relative spectrum, although in the present calculation the effect is not as huge as noted in e.g. Ref. [51].

The first difference between the two minimization schemes are in the absolute binding energies as reported in Table IV. Minimizing all the states provides solutions with lower bindings which are, in addition, in excellent agreement with the full mesh diagonalization. The second difference that we observe is in the state decomposition in the (β, γ) plane. In Figures 2a), 2b) and 2c), for illustration, we show the contributions of CHF basis vectors into the ground state wave function in the potential energy surface of $\langle \hat{J}_z \rangle = 0$. By comparing the figures 2a) and 2b), it is worth pointed out that the two minimizations produce two sets of basis vectors which

give energy spectra and transitions of the same quality. The contributions of CHF states in the figure 2b) are somehow fragmented into other configurations in the figure 2a). The effect is even more visible in the full mesh calculation shown in the figure 2c1), which means there is a redistribution of contributions in the final wave function when one uses "redundant" basis states. Now, what we observe in the figure 2c2) is the key point: the dominant CHF configurations in the full mesh diagonalization are lying in the same region as in the minimization. In Table III, we report some of the most dominant configurations in the ground state as shown in Figure 2. The most important configurations are around the Hartree-Fock minimum and they appear in both minimization calculations. In the full mesh calculation, apart from a scaling effect due to the presence of many other states, it is the same CHF configurations which contribute the most. This clearly shows that our minimization method picks up the "right" physical configurations of the most importance. This comparison also explains the reason why the minimization using 6 states gives already a good description.

We summarize now the essential points which can be drawn from the present discussion:

- i) There can be different sets of CHF states that provide the same description of the relative energy spectra and transitions.
- ii) There exists specific CHF states that contribute more significantly than others. And the minimization tells us where to find them.
- iii) One must pay attention to the interpretation because of i), it is possible to replace some set of basis states with an other, although it could be at the price of taking into account more basis states than necessary.
- iv) It is more advantageous to perform the minimization than the full mesh diagonalization since basis states are interdependent in the sense of iii). In cases where such calculation is feasible like in the present one, the full mesh diagonalization should expose the limit one obtains in the minimization. By the way, it is worth noting here that in a calculation from Monte-Carlo Shell Model of Ref. [52] employing a stochastic sampling method to choose basis states, 800 Hartree-Fock states stochastically chosen give -86.91 MeV of ground state binding for ^{24}Mg (versus the exact value -87.08 MeV) with the USD interaction.
- v) Finally, let us comment on a technical point regarding the choice of ϵ defining the convergence criterion of the method. For the present study, we use $\epsilon = 1$ keV. Such value seems to be too strict but is necessary to push the method to its limit and to see whether it reproduces the exact SM result. For that goal, this value is sufficient to avoid linear redundancies in the selection of CHF states. The redundancies among non-orthogonal states are very well known in the generator coordinate method and resulting from the nearly zero norm eigenvalues of the overlap matrix. In the minimization process, they manifest themselves through very tiny contributions in energy of order $\lesssim 10^{-1}$ keV. We therefore exclude basis

states yielding those negligible contributions.

β	γ	$\mathcal{P}_\alpha^{(J)}(\beta, \gamma)$ (%)		
		a) ground-state	b) Many-state	c) Full
0.499	12.0	5.62	7.43	1.16
0.540	17.74	14.35	15.58	2.97
0.540	11.85	4.71	14.64	1.30
0.414	17.74	7.28	-	1.44
0.351	23.63	5.25	-	1.23
0.414	11.85	3.88	7.54	0.66
0.414	29.52	-	3.39	0.61
0.477	17.74	-	-	1.38
0.477	23.63	-	-	1.29

Table III: Contributions of CHF basis states (calculated from (24)) into the ground state wave function in three calculations shown in Figure 2a), 2b) and 2c) respectively.

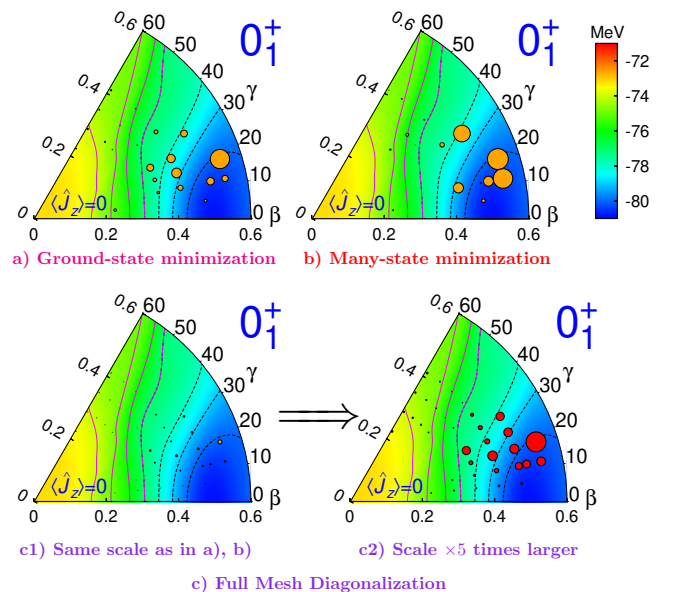


Figure 2: Structure of the ground state depicted in the potential energy surface of $\langle \hat{J}_z \rangle = 0$. The yellow circles (defined with the same scale) in a), b) and c1) represent the contribution of CHF basis vectors used in the ground-state minimization, the many-state minimization and the full mesh diagonalization respectively. In c2) the red circles represent the same CHF basis vectors of c1) but using a scaling factor of 5 times larger (see discussion in texts).

J_α^π	0_1^+	2_1^+	4_1^+	6_1^+	8_1^+
Figure 3c)	-86.828	-85.288	-82.430	-78.508	-75.028
Figure 3d)	-86.861	-85.353	-82.489	-78.619	-75.283
Figure 3e)	-86.831	-85.322	-82.483	-78.580	-75.249

J_α^π	2_2^+	3_1^+	4_2^+	5_1^+	6_2^+	7_1^+
Figure 3c)	-82.713	-81.647	-80.744	-78.905	-77.274	-74.576
Figure 3d)	-82.748	-81.695	-80.869	-79.018	-77.351	-74.661
Figure 3e)	-82.761	-81.724	-80.843	-78.992	-77.370	-74.677

Table IV: Comparison of binding energies (in MeV) obtained from the minimization of the ground state, of many states and the full mesh diagonalization in Figures 3c), 3d) and 3e) respectively.

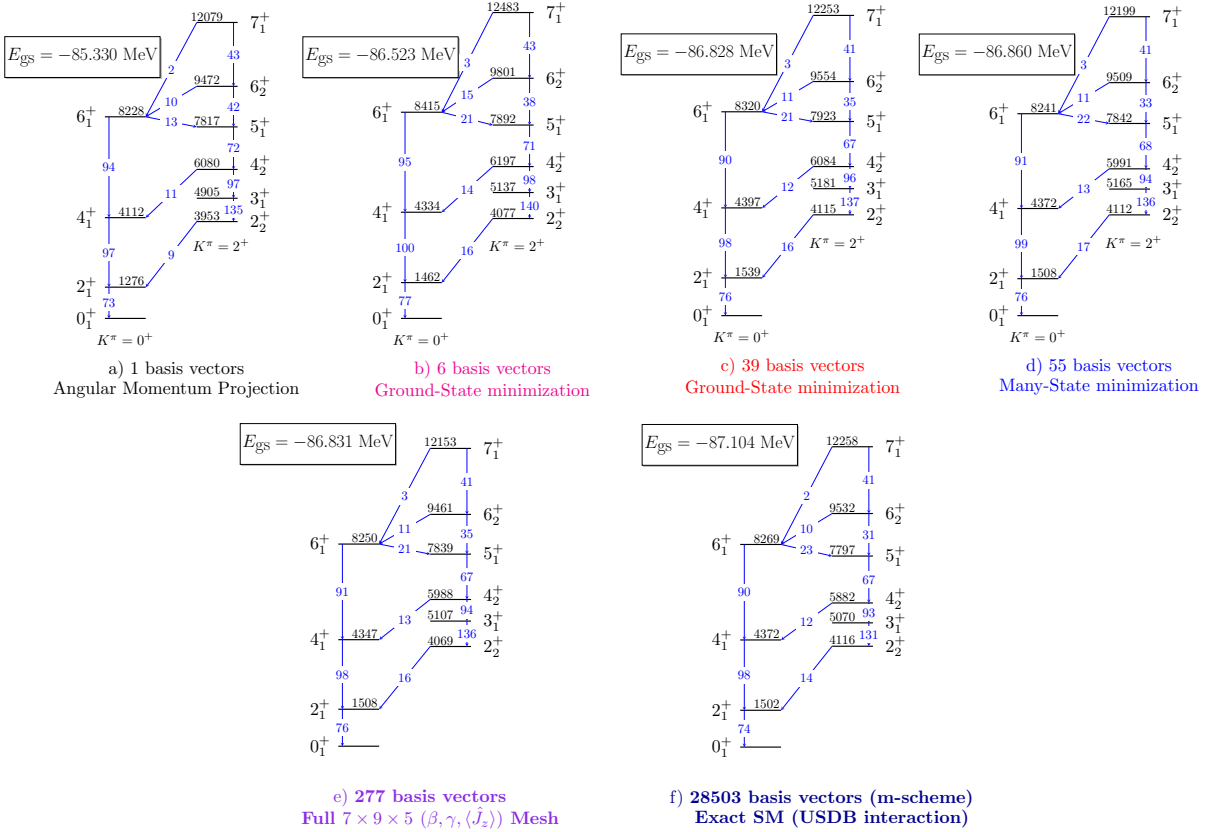


Figure 3: ^{24}Mg spectrum calculated with the USDB interaction using the DNO-SM compared to the classic SM diagonalization. Black numbers are relative energies (in keV) and blue ones the $B(E2)$ values (in $e^2 \cdot \text{fm}^4$). K denotes the dominant wave-function component of different members of the band. Figures on top show the evolution of the energy spectra between a) the Angular Momentum Projection of the Hartree-Fock minimum, b) and c) the minimization of the ground state, and d) the minimization of all considered states. Figures at bottom present e) the DNO-SM diagonalization in the full $7 \times 9 \times 5$ ($\beta, \gamma, \langle \hat{J}_z \rangle$) mesh (see texts) and f) the exact SM diagonalization. The ground state binding energy (E_{gs}) is also given for comparison.

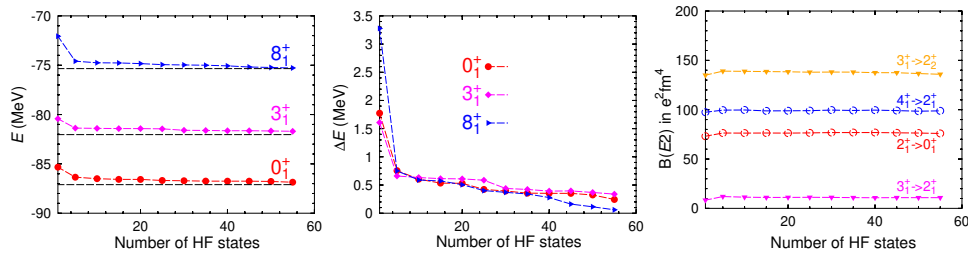


Figure 4: Convergence of the binding energies (E) (top left) where the horizontal lines represent the exact SM values, the binding energy difference (ΔE) (top right) with respect to the exact SM result and the $B(E2)$ transitions (bottom) as a function of CHF states in the many-state minimization shown in Figure 3d).

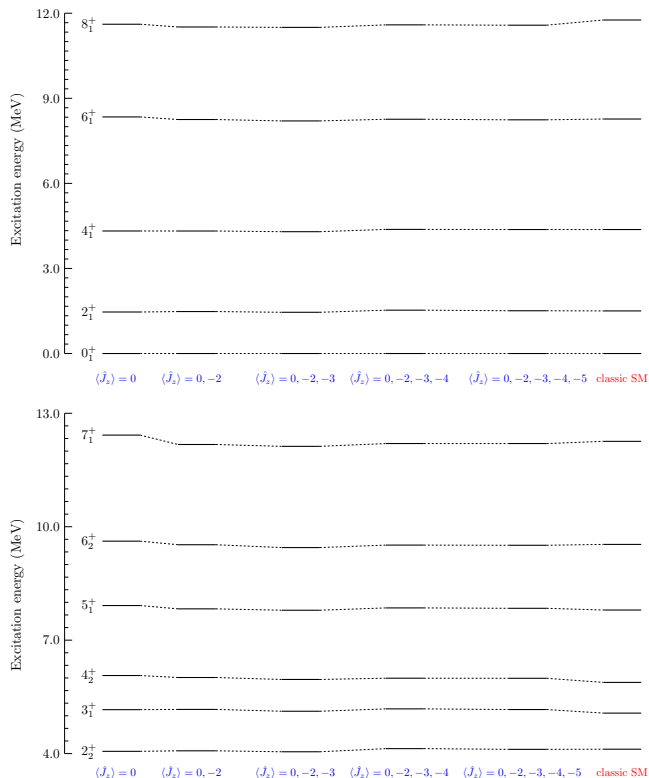


Figure 5: Evolution of the ground state band (top) and the γ -band (bottom) in ^{24}Mg as cranked CHF states are added in the many-state minimization of Figure 3d).

To look further now into the convergence process, we present in Figure 4 the evolution of absolute binding energies, the energy difference with respect to the exact SM result and the transitions as a function of the number of CHF states found in the many-state minimization of Figure 3d). The intraband and interband transitions converge after about ~ 5 iterations. In binding energies, the excited state 8_1^+ approaches the exact binding value more rapidly than the ground state. This is the effect of cranked CHF configurations and is consistent with the slight compression of the energy spectra observed in Figure 3d), Figure 5 and Table 5.

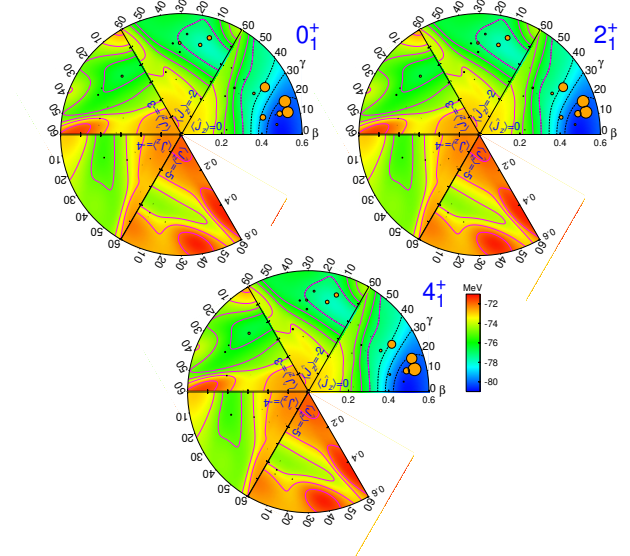


Figure 6: Structure of the first three yrast states 0_1^+ , 2_1^+ and 4_1^+ in the sextant $\gamma \in [0, 60^\circ]$ of the (β, γ) plane.

In Figures 6 and 7, the deformation structure of the yrast and the γ -band first three states is visualized in the potential energy surfaces calculated with all cranking components $\langle J_z \rangle \in \{0, -2, -3, -4, -5\}$. As already shown in Figure 2, we see now in the full decomposition, the most important states emerge from the triaxial region around the Hartree-Fock minimum.

Physically, the triaxiality developing here is often interpreted as originating from the K -mixing nature of the ground state [41]. This feature can be understood from the wave function analysis in K -quantum numbers as presented in Figure 8 where contributions from particular K -components are calculated by (24). Indeed, by construction single- K wave functions are fully preserved by the axial constraint. The small K -mixing we observe in this analysis hence reflects the deviation from a pure axial picture and therefore signal the presence of triaxial configurations which we have previously analyzed. This

mixing via the $K = 0, 2$ components also explains the weak interband transitions observed in the $B(E2)$ values.

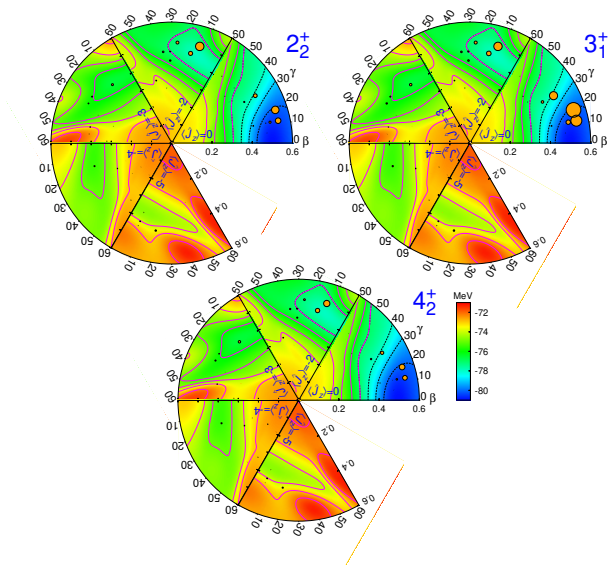


Figure 7: Structure of the first three states in the γ -band 2_2^+ , 3_1^+ and 4_2^+ in the sextant $\gamma \in [0, 60^\circ]$ of the (β, γ) plane.

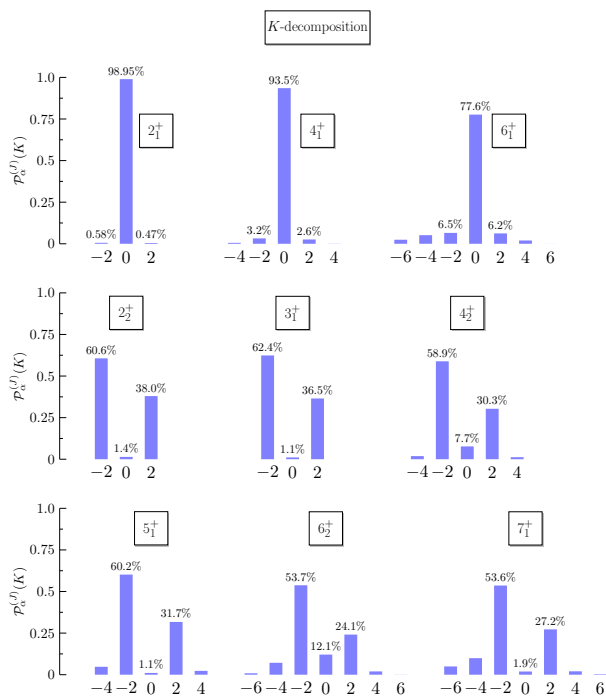


Figure 8: Decomposition of states into K -quantum numbers in ^{24}Mg

As a conclusion, the analysis of the wave function structures of ^{24}Mg shows quantitatively the intimate con-

nection between the development of triaxiality and K -mixing presences from a microscopic calculation using an underlying effective interaction. The ground state K -mixing is identified as the origin of the so-called γ -band assigned in this nucleus from geometrical models [41]. This is highly non-trivial but expected given the quality of the USDB interaction in this mass region.

C. Odd nuclei: example of ^{25}Mg

The above systematic benchmark has shown our DNO-SM's efficiency compared to the classic SM in even nuclei. As previously mentioned, the present framework is also capable to deal with odd nuclei in the same way without further treatments of the odd particle at the Hartree-Fock level. We find that the cranking Hartree-Fock can provide an excellent approach to set up the initial set of PCHF states from which we construct the basis Γ_0 through the diagonalization-minimization process. To illustrate this, we present a DNO-SM calculation of ^{25}Mg whose spectrum appears in Figure 9 compared to the classic SM one. This nucleus is known to have for instance two distinct bands: the ground state band of $K = 5/2$ and an excited band of $K = 1/2$. Employing the USDB effective interaction, this assignment is clearly seen in the wave function structure of each member of the bands as shown in Figure 10. The minimization is carried out with a discretization of 7 points $\beta \in [0.1, 0.51]$, 8 points $\gamma \in [1.5^\circ, 60^\circ]$ and with cranking components $\langle \hat{J}_z \rangle = -1/2, -3/2, -5/2, -7/2, -9/2$. The spectrum of two bands is reproduced remarkably well with a rms error of 44 keV, using 61 CHF states. The ground state binding energy is found to be -93.89 MeV versus -94.40 MeV in the exact SM result.

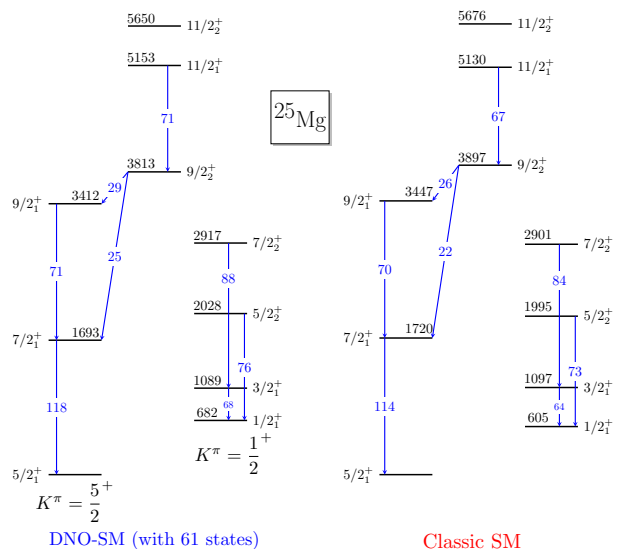


Figure 9: ^{25}Mg spectrum

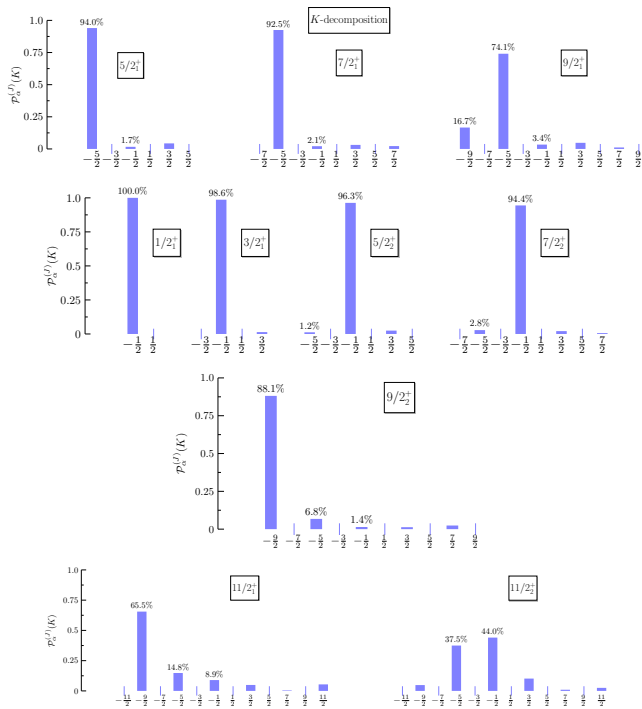


Figure 10: Decomposition of states into K -quantum numbers in ^{25}Mg

In summary for the systematic comparison we have performed between the classic exact SM and our newly developed DNO-SM, we give now a brief account of its main features as well as related questions that remain to be answered

(i) Our DNO-SM formalism is composed of three elements: the existence theorem of discrete non-orthogonal bases exposed in (6), the truncation scheme provided by the minimization technique and the diagonalization technique from the GCM theory. While the latter has been already well documented in the literature, the first element is the most important piece from the formal point of view (thanks to Ref. [26]) because it provides us a formal language to express the Shell Model in a natural way with an emphasis on the different representations of the effective Hamiltonian.

(ii) Our minimization technique has proved to be a very efficient truncation scheme in the build-up of our non-orthogonal many-body basis for the Shell Model. In all considered nuclei, a very few number of HF states is needed to obtain solutions with very good agreement with the exact SM result.

(iii) The procedure constructs the full representation of the effective Hamiltonian in an iterative way where we observe that DNO-SM solutions are closer and closer from the above to the exact diagonalization limit: $\mathcal{H}_q \rightarrow \mathcal{H}$, which means our DNO-SM is an approximation (given some particular choice of the coordinate(s) q) to the classic SM. This point merits to be mentioned because it points out the need to design a theoretical approach to choose the coordinate(s) q if one wants to ob-

tain the full representation of the effective Hamiltonian. Whether this question can be formally demonstrated *a priori* without numerical calculations is an interesting problem to investigate.

(iv) The wave functions and excitation energies converge faster than the absolute energy. As depicted in Figure 1, there's some missing energy in the ground state ranging around 50 – 900 keV depending on specific cases. However, it has practically no impacts on the wave functions because transition probabilities are already very well reproduced (cf. Table II). The physical origin of this missing binding energy is very likely related to (iii), i.e. the choice of q . Here we would like to mention that the multipolarity decomposition of the effective Hamiltonian designed by A. Zuker *et al.* (see e.g. Ref. [1]) could be instrumental to investigate both (iii) and (iv).

(v) Lastly, the present framework is capable to treat equally well even- and odd-mass nuclei where the cranking method is found to be really efficient in the construction of the many-body basis.

To conclude, it is worth noting that the energy difference we have found using the PCHF basis is of the same order and consistent with what have been reported in similar studies of Refs. [21, 22, 53, 54] where more sophisticated trial wave functions of Hartree-Fock-Bogoliubov (HFB) types with pairing correlations included explicitly are used (see e.g. Figure 8 of Ref. [22]). Finally, let us mention that our definition of (β, γ) is the same as in Refs. [21, 22] up to a factor of effective charge $e_{mass}^{(p)} = e_{mass}^{(n)}$. For example, in ^{24}Mg , omitting the effective charge would yield $\beta = 0.499/1.77 \approx 0.282$ which agrees well with Ref. [21] (cf. Table 1 therein). We would like however to keep this effective charge factor for defining mass quadrupole moments to be able to compare with β_2 -values extracted from experimental electric BE(2) transitions which yield, e.g. 0.605 in ^{24}Mg .

IV. A FIRST SHELL MODEL CALCULATION OF ^{254}No

The quest for superheavy elements is a subject under intensive experimental investigations and usually, the predictions for the shell stabilization of the superheavy elements predictions rely essentially on "standard" mean-field calculations. In the following, we will apply the DNO-SM method to illustrate its applicability in the context of superheavy systems and we propose here for the first time, a shell-model type of description of ^{254}No superheavy nucleus, using the DNO-SM. The shell-model valence space is spanned by the full Z=82-126 proton major shell and the full N=126-184 neutron major shell beyond ^{208}Pb , namely, the single proton orbitals $0h_{\frac{9}{2}}$, $1f_{\frac{7}{2}}$, $0i_{\frac{13}{2}}$, $1f_{\frac{5}{2}}$, $2p_{\frac{3}{2}}$, $2p_{\frac{1}{2}}$, and the single neutron orbitals $1g_{\frac{9}{2}}$, $0i_{\frac{11}{2}}$, $0j_{\frac{15}{2}}$, $2d_{\frac{5}{2}}$, $3s_{\frac{1}{2}}$, $1g_{\frac{7}{2}}$, $2d_{\frac{3}{2}}$ (the valence space is illustrated in in Fig. 11). As effective interaction, we use the modified Kuo-Herling realistic interaction (see [55] for

details) which was applied with great success along the $N=126$ isotones [55, 56]. The single particle energies are borrowed from ^{209}Bi and ^{209}Pb spectra for protons and neutrons respectively. The electric polarization charge here is taken to be $\chi_p = \chi_n = 0.5$.

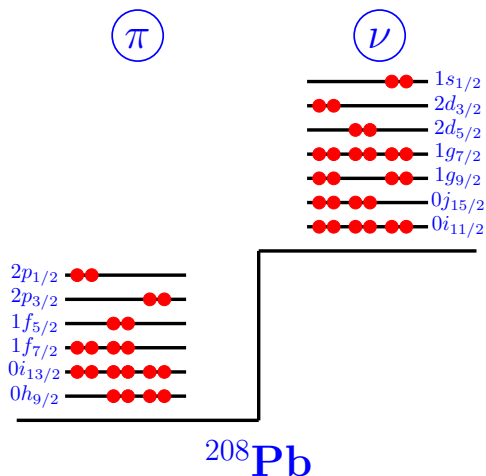


Figure 11: Valence space above ^{208}Pb

^{254}No is a deformed nucleus whose spectroscopy has been intensively investigated the recent years. In addition to the observation of its rotational Yrast structure, a side $K = 3+$ band and two long lived isomers have been observed [57, 58]. Figure 12 shows the potential energy surface obtained for the mass (β, γ) deformation parameters (obtained from the mass quadrupole moments defined in section II C 3). The deformation landscape shows a clear prolate axial minimum around $\beta \sim 0.2$ extending moderately towards non-axial shapes.

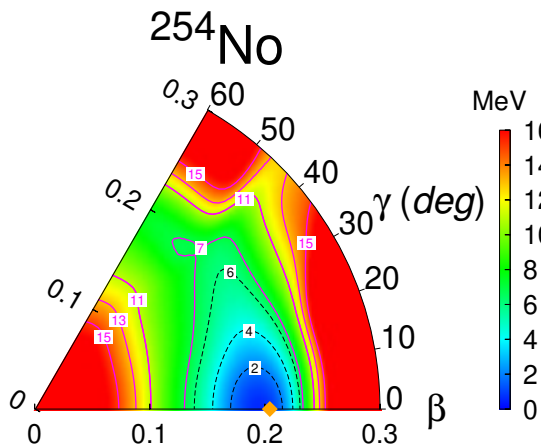


Figure 12: Potential Energy Surface (PES) of ^{254}No calculated with the Kuo-Herling effective interaction where the yellow diamond is the axial HF minimum with the mass quadrupole parameter $\beta = 0.2$.

All the considered states are calculated with the minimization technique over a restricted region around the corresponding HF minimum. The spectrum of ^{254}No resulting from these calculations is shown in figure 13 as the function of the number of HF states retained by the minimization procedure. With a relatively small number of basis states, we observe a fast and good convergence of the low-lying members of the Yrast band but also for the higher lying isomer 8^- isomer. As already shown in the previous section, the DNO-SM allows analysis of the states under study in terms of intrinsic quantities, namely, deformations (β, γ) and the intrinsic angular momentum. The whole low-lying spectrum is presented in figure 14. The various states are shown and grouped in 3 structures: a $K^\pi = 0^+$ Yrast rotational band, a $K^\pi = 3^+$ multiplet and the $K^\pi = 8^-$ state. There is an excellent agreement for the reproduction of the Yrast rotational sequence, and the 8^- isomeric state. The 3^- state bandhead of the $K = 3$ multiplet is lying a little bit too low, by the interband spacing is also very well reproduced. The formalism allows to extract the fractional spherical occupancies of the orbitals in the valence space. The structure of the three 0_1^+ , 3_1^+ and 8_1^- states is shown in Table V. with a possible large mixing of spherical orbital our description is richer than single quasi-particle estimates which are often used to assign excited and isomeric states to a single excited configurations. This is reflected in the partial occupancies of the whole proton and neutron orbitals involved in the valence space. Nevertheless, one can point out that both for protons and neutrons, the fillings proceed through the "largest" orbitals and that excited 3_1^+ and 8_1^- states mainly differ from the ground state by an additional proton particle filling the $1h_{9/2}$ orbital, assigning these states as having a "proton" nature. We may recall here that we obtain an excellent reproduction of the experimental data with no adjustment of the effective interaction, designed more than two decades ago. Nevertheless, in order to confirm the present outcome from our calculations, a broader systematic study has been developed, and in particular we would like to connect the slight energy shift of the $K^\pi = 3^+$ multiplet to a specific single particle monopole drift for a better reproductive and predictive description of the overall region.

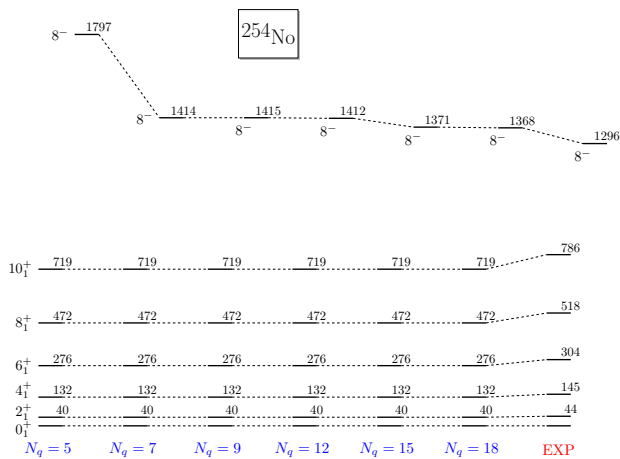


Figure 13: Evolution of the lower part of ^{254}No spectrum with respect to the number of HF states found by the minimization procedure.

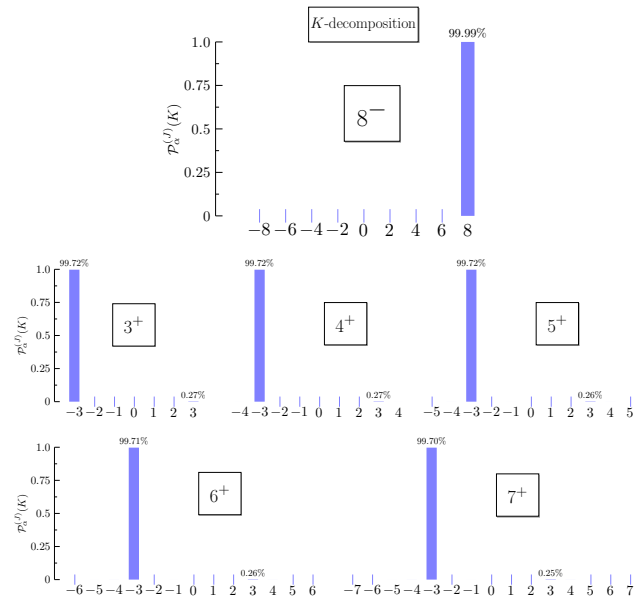


Figure 15: K -quantum number content of the isomeric 3^+ band and the 8^- state.

proton orbits	$1h_{9/2}$	$1i_{13/2}$	$2f_{7/2}$	$2f_{5/2}$	$3p_{3/2}$	$3p_{1/2}$	
0_1^+	5.66	7.99	3.44	1.58	0.76	0.57	
8^-	6.52	7.82	3.28	1.20	0.79	0.39	
3^+	6.50	7.98	3.31	1.14	0.72	0.35	
neutron orbits	$1i_{11/2}$	$1j_{15/2}$	$2g_{9/2}$	$2g_{7/2}$	$3d_{5/2}$	$3d_{3/2}$	$4s_{1/2}$
0_1^+	7.28	9.67	5.45	1.11	1.16	0.87	0.46
8^-	7.29	9.04	6.07	1.12	1.15	0.88	0.45
3^+	7.31	9.94	5.43	0.99	1.07	0.83	0.43

Table V: Occupancies of the spherical orbitals for the ground state and 8^- and 3^+ states.

V. CONCLUSION AND PERSPECTIVES

As a summary, in this paper we have exposed the formalism of the DNO-SM which amounts to diagonalize shell-model hamiltonians in a non-orthogonal basis with the use of beyond-mean-field techniques. Particular effort has been put into the proper selection of optimal basis state used for the diagonalisation. We benchmarked the method over a large set of sd shell nuclei and could reproduce the energies, and transitions probabilities of the exact diagonalisations with minimal cost of very few basis states. For the first time, we applied the DNO-SM method to a superheavy system ^{254}No which is obviously far beyond the capabilities of actual diagonalisation codes. The DNO-SM formalism has also recently been very useful in the interpretation of several experimental studies [59–62] and has been to be extremely promising both for intrinsic interpretation of shell-model

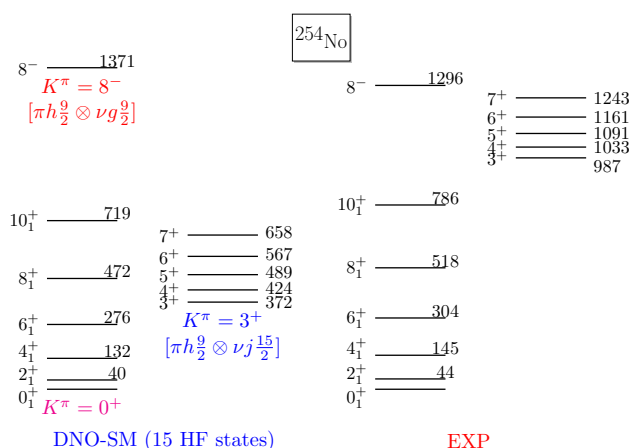


Figure 14: Comparison of DNO-SM calculation using 15 HF states with the experimental spectrum.

diagonalisations, and setting new frontiers for nuclear structure studies within the shell-model framework.

VI. ACKNOWLEDGMENTS

The authors would like to dedicate the present work to the memory of the late Etienne Caurier, who was at the initiative of the present developments.

Appendix A: Matrix elements in the PCHF basis

Considering the two-body Hamiltonian $\hat{\mathcal{H}}$ defined in (2), in the PCHF basis $\mathcal{P}_{MK}^J|\Phi(q)\rangle \in \Gamma_0$, it is repre-

$$\langle\Phi'|\hat{\mathcal{H}}\hat{R}(\Omega)|\Phi\rangle = \sum_{\substack{p\in\Phi' \\ q\in\Phi}} (-)^{p+q} M_{pq}(\Omega) \langle p|\hat{E}\hat{R}(\Omega)|q\rangle + \sum_{\substack{p<q\in\Phi' \\ r<s\in\Phi}} (-)^{p+q+r+s} M_{pqrs}(\Omega) \langle pq|\hat{\mathcal{V}}\hat{R}(\Omega)|rs\rangle \quad (\text{A1})$$

where $M_{pq}(\Omega), M_{pqrs}(\Omega)$ are respectively first- and second-order minors of the $A \times A$ matrix $N(\Omega) = D'^{\dagger} \cdot R(\Omega) \cdot D$ with a rectangular matrix $D_{ip} = \{C_i^{(p)}, p \in \Phi, i \in \mathcal{E}\}$ representing the single particle HF states in the Slater $|\Phi\rangle$. $C_i^{(p)}$ represents here the expansion coefficient of the single-particle Hartree-Fock state $|p\rangle$ in the single-particle Harmonic Oscillator basis $\{|i\rangle\}$. The matrix element of the one-body single-particle energy \hat{E} is given by

$$\langle p|\hat{E}\hat{R}(\Omega)|q\rangle = \sum_{i_1, i_2, i \in \mathcal{E}} C_{i_1}^{(p)} C_{i_2}^{(q)} e_{i_1 i} R_{i i_2}(\Omega). \quad (\text{A2})$$

$$\langle pq|\hat{\mathcal{V}}\hat{R}(\Omega)|rs\rangle = \sum_{\substack{JMM' \\ TT_z \\ i_1 i_2 i_3 i_4}} C_{\frac{1}{2}\tau_p \frac{1}{2}\tau_q}^{TT_z} C_{\frac{1}{2}\tau_r \frac{1}{2}\tau_s}^{TT_z} C_{j_1 m_1 j_2 m_2}^{JM} C_{j_3 m_3 j_4 m_4}^{JM'} \mathcal{D}_{MM'}^J(\Omega) C_{i_1}^{(p)} C_{i_2}^{(q)} C_{i_3}^{(r)} C_{i_4}^{(s)} \langle JT(i_1 i_2)|\hat{\mathcal{V}}|JT(i_3 i_4)\rangle. \quad (\text{A3})$$

Here $C_{j_1 m_1 j_2 m_2}^{JM}$ is the Clebsch–Gordan coefficient.

Appendix B: Derivation of the analytical integration over the Euler angles α, γ

Appendix A provides the necessary elements we need to derive an analytical formula for the integrations over α, γ in (16). For that goal, we just need to perform the derivation with $\hat{\mathcal{O}} = \mathbf{1}$, the same procedure holds for other operators such as the Hamiltonian or transition

operators. In this case, we have the norm matrix element

$$\mathcal{N}_{K'K}^J = \frac{2J+1}{4\pi^2(3-(-)^A)} \int d\Omega \mathcal{D}_{MK}^{J*}(\Omega) \det N(\Omega) \quad (\text{B1})$$

where we have used the equality $\det N(\Omega) = \langle\Phi'|\hat{R}(\Omega)|\Phi\rangle$. Let us rewrite this quantity in an explicit way with a summation over all permutations σ of the

permutation group of A -particles S_A

$$\begin{aligned}
\det N &= \sum_{\sigma \in S_A} \text{sgn}(\sigma) \prod_{\lambda=1}^A N_{\lambda, \sigma(\lambda)} \\
&= \sum_{\sigma \in S_A} \text{sgn}(\sigma) \prod_{\lambda=1}^A \left(\sum_{i_1 i_2 \in \mathcal{E}} D'_{\lambda i_1} R_{i_1 i_2} D_{i_2 \sigma(\lambda)} \right) \\
&= \sum_{\substack{i_1(1) i_2(1) \\ \dots \\ i_1(A) i_2(A)}} \prod_{\lambda=1}^A D'_{\lambda i_1(\lambda)} \prod_{\lambda=1}^A R_{i_1(\lambda) i_2(\lambda)} \\
&\quad \left(\sum_{\sigma \in S_A} \text{sgn}(\sigma) \prod_{\lambda=1}^A D_{i_2(\lambda) \sigma(\lambda)} \right). \tag{B2}
\end{aligned}$$

The norm matrix element thus becomes

$$\begin{aligned}
\mathcal{N}_{K'K}^{(J)} &= \frac{2J+1}{4\pi^2(3-(-)^A)} \sum_{\substack{i_1(1) i_2(1) \\ \dots \\ i_1(A) i_2(A)}} \\
&\quad \prod_{\lambda=1}^A D'_{\lambda i_1(\lambda)} \left(\sum_{\sigma \in S_A} \text{sgn}(\sigma) \prod_{\lambda=1}^A D_{i_2(\lambda) \sigma(\lambda)} \right) \times \\
&\quad \int d\Omega \mathcal{D}_{MK}^{J*}(\Omega) \prod_{\lambda=1}^A R_{i_1(\lambda) i_2(\lambda)}(\Omega). \tag{B3}
\end{aligned}$$

In this form, the integration over Euler angles $\Omega = (\alpha, \beta, \gamma)$ is isolated and can be subject to a direct evaluation using the rotation matrix in spherical oscillator basis $R_{i_1 i_2}(\Omega) = e^{-i\alpha m_1} d_{m_1 m_2}^j(\beta) e^{-i\gamma m_2}$. Hence, one can write

$$\begin{aligned}
&\int d\Omega \mathcal{D}_{MK}^{J*}(\Omega) \prod_{\lambda=1}^A R_{i_1(\lambda) i_2(\lambda)}(\Omega) \\
&= \int_0^{2\pi} d\alpha e^{i\alpha [K' - \sum_{\lambda=1}^A m_1(\lambda)]} \int_0^{\gamma_{\max}} d\gamma e^{i\gamma [K - \sum_{\lambda=1}^A m_2(\lambda)]} \\
&\quad \int_0^\pi d\beta \sin \beta d_{K'K}^{*J}(\beta) \prod_{\lambda=1}^A d_{m_1(\lambda) m_2(\lambda)}^{j(\lambda)}(\beta) \tag{B4}
\end{aligned}$$

from which it is trivial to calculate the integrals over α, γ . The result simply reads

$$\begin{aligned}
&\int d\Omega \mathcal{D}_{MK}^{J*}(\Omega) \prod_{\lambda=1}^A R_{i_1(\lambda) i_2(\lambda)}(\Omega) = 2\pi \gamma_{\max} \times \\
&\quad \delta_{\Delta K', 0} \delta_{\Delta K, 0} \int_0^\pi d\beta \sin \beta d_{K'K}^{*J}(\beta) \prod_{\lambda=1}^A d_{m_1(\lambda) m_2(\lambda)}^{j(\lambda)}(\beta) \tag{B5}
\end{aligned}$$

where we denote $\Delta K' = K' - \sum_{\lambda=1}^A m_1(\lambda)$ and $\Delta K = K - \sum_{\lambda=1}^A m_2(\lambda)$. This form is of course not practical as it involves summations over $A!$ permutations. Our next step is to recast it into the familiar expression as in (B1) with only the integration over β being left to evaluate. To do so, notice that

$$\delta_{n,0} = \frac{1}{N} \sum_{k=1}^N e^{i \frac{2\pi k}{N} n} \text{ if } \begin{cases} N \in \mathbb{N}, N \geq 2, \\ n \in \mathbb{Z}, e^{i \frac{2\pi}{N} n} \neq 1. \end{cases} \tag{B6}$$

It is obvious that $\Delta K', \Delta K \in \mathbb{Z}$ regardless the odd or even mass number A so that applying this identity allows us to obtain

$$\begin{aligned}
&\int d\Omega \mathcal{D}_{MK}^{J*}(\Omega) \prod_{\lambda=1}^A R_{i_1(\lambda) i_2(\lambda)}(\Omega) = \frac{2\pi \gamma_{\max}}{N_\alpha N_\gamma} \times \\
&\quad \sum_{k_1=1}^{N_\alpha} \sum_{k_2=1}^{N_\gamma} \int_0^\pi d\beta \sin \beta \mathcal{D}_{K'K}^{*J} \left(\frac{2\pi k_1}{N_\alpha}, \beta, \frac{2\pi k_2}{N_\gamma} \right) \times \\
&\quad \prod_{\lambda=1}^A R_{i_1(\lambda) i_2(\lambda)} \left(\frac{2\pi k_1}{N_\alpha}, \beta, \frac{2\pi k_2}{N_\gamma} \right) \tag{B7}
\end{aligned}$$

where $N_\alpha, N_\gamma \in \mathbb{Z}$ are chosen according to the condition (B6). The final expression of the norm matrix element thus reads

$$\begin{aligned}
\mathcal{N}_{K'K}^J &= \frac{2J+1}{2} \cdot \frac{1}{N_\alpha N_\gamma} \sum_{k_1=1}^{N_\alpha} \sum_{k_2=1}^{N_\gamma} \int_0^\pi d\beta \sin \beta \times \\
&\quad \mathcal{D}_{K'K}^{*J} \left(\frac{2\pi k_1}{N_\alpha}, \beta, \frac{2\pi k_2}{N_\gamma} \right) \times \det N \left(\frac{2\pi k_1}{N_\alpha}, \beta, \frac{2\pi k_2}{N_\gamma} \right). \tag{B8}
\end{aligned}$$

The same reasoning leaves us with the Hamiltonian matrix element where α, γ are exactly integrated out

$$\mathcal{H}_{K'K}^J = \frac{2J+1}{2} \cdot \frac{1}{N_\alpha N_\gamma} \sum_{k_1=1}^{N_\alpha} \sum_{k_2=1}^{N_\gamma} \int_0^\pi d\beta \sin \beta \mathcal{D}_{K'K}^{*J} \left(\frac{2\pi k_1}{N_\alpha}, \beta, \frac{2\pi k_2}{N_\gamma} \right) \langle \Phi' | \hat{\mathcal{H}} \hat{R} \left(\frac{2\pi k_1}{N_\alpha}, \beta, \frac{2\pi k_2}{N_\gamma} \right) | \Phi \rangle. \quad (\text{B9})$$

$N_u (u = \alpha, \gamma)$ will be chosen to ensure the conditions

$$e^{i \frac{2\pi}{N_u} \Delta K_v} \neq 1 \quad \forall v = 0, 1, 2 \text{ with } \begin{cases} \Delta K_0 = K - \sum_{\lambda=1}^A m_i(\lambda) & \forall i \in \mathcal{E} \\ \Delta K_1 = K - m_i - \sum_{\lambda=1}^{A-1} m_{i'}(\lambda) & \forall i, i' \in \mathcal{E} \\ \Delta K_2 = K - M(i_1, i_2) - \sum_{\lambda=1}^{A-2} m_i(\lambda) & \forall i, i_1, i_2 \in \mathcal{E} \end{cases} \quad (\text{B10})$$

with i_1, i_2 designating two single-particle harmonics oscillator states coupled to a total angular momentum

$$M = m_{i_1} + m_{i_2}.$$

-
- [1] E. Caurier, G. Martínez-Pinedo, F. Nowacki, A. Poves, and A. P. Zuker, *Rev. Mod. Phys.* **77**, 427 (2005), URL <https://link.aps.org/doi/10.1103/RevModPhys.77.427>.
- [2] F. Nowacki, A. Obertelli, and A. Poves, *Progress in Particle and Nuclear Physics* **120**, 103866 (2021), ISSN 0146-6410, URL <https://www.sciencedirect.com/science/article/pii/S014664102100020X>.
- [3] E. Caurier, G. Martínez-Pinedo, F. Nowacki, A. Poves, J. Retamosa, and A. P. Zuker, *Phys. Rev. C* **59**, 2033 (1999), URL <https://link.aps.org/doi/10.1103/PhysRevC.59.2033>.
- [4] F. Nowacki, A. Poves, E. Caurier, and B. Bounthong, *Phys. Rev. Lett.* **117**, 272501 (2016), URL <https://link.aps.org/doi/10.1103/PhysRevLett.117.272501>.
- [5] C. Hinke, M. Böhmer, P. Boutachkov, et al., *Nature* **341**, 341 (2012).
- [6] M. Siciliano, J. Valiente-Dobón, A. Goasduff, F. Nowacki, A. Zuker, D. Bazzacco, A. Lopez-Martens, E. Clément, G. Benzoni, T. Braunroth, et al., *Physics Letters B* **806**, 135474 (2020), ISSN 0370-2693, URL <https://www.sciencedirect.com/science/article/pii/S0370269320302781>.
- [7] D. Rosiak, M. Seidlitz, P. Reiter, H. Naïdja, Y. Tsunoda, T. Togashi, F. Nowacki, T. Otsuka, G. Colò, K. Arnsward, et al. (MINIBALL and HIE-ISOLDE Collaborations), *Phys. Rev. Lett.* **121**, 252501 (2018), URL <https://link.aps.org/doi/10.1103/PhysRevLett.121.252501>.
- [8] H. Naïdja, F. Nowacki, and B. Bounthong, *Phys. Rev. C* **96**, 034312 (2017), URL <https://link.aps.org/doi/10.1103/PhysRevC.96.034312>.
- [9] M. Bender, P.-H. Heenen, and P.-G. Reinhard, *Rev. Mod. Phys.* **75**, 121 (2003), URL <https://link.aps.org/doi/10.1103/RevModPhys.75.121>.
- [10] J. L. Egido, *Physica Scripta* **91**, 073003 (2016), URL <https://doi.org/10.1088/0031-8949/91/7/073003>.
- [11] L. M. Robledo, T. R. Rodríguez, and R. R. Rodríguez-Guzmán, *Journal of Physics G: Nuclear and Particle Physics* **46**, 013001 (2018), URL <https://doi.org/10.1088/1361-6471/aadebd>.
- [12] G. Ripka, *Lectures in Theoretical Physics: Volume VIII C* (The University of Colorado Press, 1965).
- [13] G. Ripka, *The Hartree-Fock Theory of Deformed Light Nuclei* (Springer US, Boston, MA, 1968), pp. 183–259.
- [14] K. W. Schmid and F. Grummer, *Reports on Progress in Physics* **50**, 731 (1987), URL <https://doi.org/10.1088/0034-4885/50/6/003>.
- [15] K. Schmid, *Progress in Particle and Nuclear Physics* **52**, 565 (2004), ISSN 0146-6410, URL <https://www.sciencedirect.com/science/article/pii/S0146641004000134>.
- [16] T. Otsuka, M. Honma, and T. Mizusaki, *Phys. Rev. Lett.* **81**, 1588 (1998), URL <https://link.aps.org/doi/10.1103/PhysRevLett.81.1588>.
- [17] Y. Utsuno, T. Otsuka, T. Mizusaki, and M. Honma, *Phys. Rev. C* **60**, 054315 (1999), URL <https://link.aps.org/doi/10.1103/PhysRevC.60.054315>.
- [18] Y. Tsunoda, T. Otsuka, N. Shimizu, M. Honma, and Y. Utsuno, *Phys. Rev. C* **89**, 031301 (2014), URL <https://link.aps.org/doi/10.1103/PhysRevC.89.031301>.
- [19] Z.-C. Gao and M. Horoi, *Phys. Rev. C* **79**, 014311 (2009),

- URL <https://link.aps.org/doi/10.1103/PhysRevC.79.014311>.
- [20] N. Hinohara and Y. Kanada-En'yo, *Phys. Rev. C* **83**, 014321 (2011), URL <https://link.aps.org/doi/10.1103/PhysRevC.83.014321>.
- [21] Bally, B., Sánchez-Fernández, A., and Rodríguez, T. R., *Eur. Phys. J. A* **57**, 69 (2021), URL <https://doi.org/10.1140/epja/s10050-021-00369-z>.
- [22] A. Sánchez-Fernández, B. Bally, and T. R. Rodríguez, *Phys. Rev. C* **104**, 054306 (2021), URL <https://link.aps.org/doi/10.1103/PhysRevC.104.054306>.
- [23] B. Bally, A. Sánchez-Fernández, and T. R. Rodríguez, *Phys. Rev. C* **100**, 044308 (2019), URL <https://link.aps.org/doi/10.1103/PhysRevC.100.044308>.
- [24] J. J. Griffin and J. A. Wheeler, *Phys. Rev.* **108**, 311 (1957), URL <https://link.aps.org/doi/10.1103/PhysRev.108.311>.
- [25] R. E. Peierls and J. Yoccoz, *Proceedings of the Physical Society. Section A* **70**, 381 (1957), URL <https://doi.org/10.1088/0370-1298/70/5/309>.
- [26] J. Broeckhove and E. Deumens, *Z. Phys. A* **292**, 243 (1979).
- [27] E. Caurier, *Proc. on GCM*, BLG report **484**, 200 (1975).
- [28] E. D. F. Arickx, J. Broeckhove and P. V. Leuven, *J. Comp. Phys.* **39**, 272 (1981).
- [29] D. D. Johnson, *Phys. Rev. B* **38**, 12807 (1988), URL <https://link.aps.org/doi/10.1103/PhysRevB.38.12807>.
- [30] V. Eyert, *Journal of Computational Physics* **124**, 271 (1996), ISSN 0021-9991, URL <https://www.sciencedirect.com/science/article/pii/S0021999196900595>.
- [31] A. Baran, A. Bulgac, M. M. Forbes, G. Hagen, W. Nazarewicz, N. Schunck, and M. V. Stoitsov, *Phys. Rev. C* **78**, 014318 (2008), URL <https://link.aps.org/doi/10.1103/PhysRevC.78.014318>.
- [32] Staszczak, A., Stoitsov, M., Baran, A., and Nazarewicz, W., *Eur. Phys. J. A* **46**, 85 (2010), URL <https://doi.org/10.1140/epja/i2010-11018-9>.
- [33] H. Lamme and E. Boeker, *Nuclear Physics A* **111**, 492 (1968), ISSN 0375-9474, URL <https://www.sciencedirect.com/science/article/pii/0375947468902352>.
- [34] A. Messiah, *Quantum mechanics* (North-Holland Publishing Co., Amsterdam, 1965).
- [35] G. Bertsch, J. Dobaczewski, W. Nazarewicz, and J. Pei, *Phys. Rev. A* **79**, 043602 (2009), URL <https://link.aps.org/doi/10.1103/PhysRevA.79.043602>.
- [36] H. Kasuya and K. Yoshida, *Prog. Theo. Exp. Phys.* **2021** (2021).
- [37] A. Watt, *J. Phys. A: Gen. Phys.* **5** (1972).
- [38] T. R. Rodríguez and J. L. Egido, *Phys. Rev. C* **81**, 064323 (2010), URL <https://link.aps.org/doi/10.1103/PhysRevC.81.064323>.
- [39] M. Bender and P.-H. Heenen, *Phys. Rev. C* **78**, 024309 (2008), URL <https://link.aps.org/doi/10.1103/PhysRevC.78.024309>.
- [40] K. Burzyński and J. Dobaczewski, *Phys. Rev. C* **51**, 1825 (1995), URL <https://link.aps.org/doi/10.1103/PhysRevC.51.1825>.
- [41] P. Ring and P. Schuck, *The Nuclear Many-Body Problem* (Springer-Verlag, Heidelberg, 1980, 1980).
- [42] D. L. Hill and J. A. Wheeler, *Phys. Rev.* **89**, 1102 (1953), URL <https://link.aps.org/doi/10.1103/PhysRev.89.1102>.
- [43] P. J. Brussard and P. W. M. Glaudemans, *Shell Model Applications in Nuclear Spectroscopy* (North-Holland Publishing Co., Amsterdam .New York. Oxford, 1977).
- [44] J. Suhonen, *From Nucleons to Nucleus, Concepts of Microscopic Nuclear Theory* (Springer-Verlag Berlin Heidelberg, 2007).
- [45] A. P. Zuker, A. Poves, F. Nowacki, and S. M. Lenzi, *Phys. Rev. C* **92**, 024320 (2015), URL <https://link.aps.org/doi/10.1103/PhysRevC.92.024320>.
- [46] L. Coraggio and N. Itaco, *Frontiers in Physics* **8** (2020), ISSN 2296-424X, URL <https://www.frontiersin.org/article/10.3389/fphy.2020.00345>.
- [47] M. Dufour and A. P. Zuker, *Phys. Rev. C* **54**, 1641 (1996), URL <https://link.aps.org/doi/10.1103/PhysRevC.54.1641>.
- [48] B. A. Brown and W. A. Richter, *Phys. Rev. C* **74**, 034315 (2006), URL <https://link.aps.org/doi/10.1103/PhysRevC.74.034315>.
- [49] J. M. Yao, J. Meng, P. Ring, and D. P. Arteaga, *Phys. Rev. C* **79**, 044312 (2009), URL <https://link.aps.org/doi/10.1103/PhysRevC.79.044312>.
- [50] J. M. Yao, J. Meng, P. Ring, and D. Vretenar, *Phys. Rev. C* **81**, 044311 (2010), URL <https://link.aps.org/doi/10.1103/PhysRevC.81.044311>.
- [51] M. Borrajo, T. R. Rodríguez, and J. Luis Egido, *Physics Letters B* **746**, 341 (2015), ISSN 0370-2693, URL <https://www.sciencedirect.com/science/article/pii/S0370269315003676>.
- [52] M. Honma, T. Mizusaki, and T. Otsuka, *Phys. Rev. Lett.* **77**, 3315 (1996), URL <https://link.aps.org/doi/10.1103/PhysRevLett.77.3315>.
- [53] J.-Q. Wang, Z.-C. Gao, Y.-J. Ma, and Y. S. Chen, *Phys. Rev. C* **98**, 021301 (2018), URL <https://link.aps.org/doi/10.1103/PhysRevC.98.021301>.
- [54] Bally, B., Sánchez-Fernández, A., and Rodríguez, T. R., *Eur. Phys. J. A* **57**, 124 (2021), URL <https://doi.org/10.1140/epja/s10050-021-00406-x>.
- [55] E. Caurier, M. Rejmund, and H. Grawe, *Phys. Rev. C* **67**, 054310 (2003), URL <https://link.aps.org/doi/10.1103/PhysRevC.67.054310>.
- [56] K. Hauschild, M. Rejmund, H. Grawe, E. Caurier, F. Nowacki, F. Becker, Y. Le Coz, W. Korten, J. Döring, M. Górska, et al., *Phys. Rev. Lett.* **87**, 072501 (2001), URL <https://link.aps.org/doi/10.1103/PhysRevLett.87.072501>.
- [57] R. Herzberg, P. Greenlees, and P. Butler, *Nature* **442**, 896–899 (2006).
- [58] R. Clark, K. Gregorich, J. Berryman, M. Ali, J. Allmond, C. Beausang, M. Cromaz, M. Deleplanque, I. Dragojević, J. Dvorak, et al., *Physics Letters B* **690**, 19 (2010), ISSN 0370-2693, URL <https://www.sciencedirect.com/science/article/pii/S0370269310005757>.
- [59] S. Calinescu, O. Sorlin, I. Matea, F. Carstoiu, D. D. Dao, F. Nowacki, G. de Angelis, R. Astabatyán, S. Bagchi, C. Borcea, et al., *Phys. Rev. C* **104**, 034318 (2021), URL <https://link.aps.org/doi/10.1103/PhysRevC.104.034318>.
- [60] K. Rezynkina et al., to be submitted to *Phys. Rev.* (2022).
- [61] D. Reygadas et al., to be submitted to *Phys. Rev.* (2022).
- [62] M. Rocchini et al., to be submitted to *Phys. Rev.* (2022).